Flexible and Highly Sensitive Strain Sensors Fabricated by Pencil Drawn for Wearable Monitor

*Xinqin Liao, Qingliang Liao, Xiaoqin Yan, Qijie Liang, Haonan Si, Minghua Li, Hualin Wu, Shiyao Cao, and Yue Zhang**

Functional electrical devices have promising potentials in structural health monitoring system, human-friendly wearable interactive system, smart robotics, and even future multifunctional intelligent room. Here, a low-cost fabrication strategy to efficiently construct highly sensitive graphite-based strain sensors by pencil-trace drawn on flexible printing papers is reported. The strain sensors can be operated at only two batteries voltage of 3 V, and can be applied to variously monitoring microstructural changes and human motions with fast response/relaxation times of 110 ms, a high gauge factor (GF) of 536.6, and high stability >10 000 bending–unbending cycles. Through investigation of service behaviors of the sensors, it is found that the microcracks occur on the surface of the pencil-trace and have a major influence on the functions of the strain sensors. These performances of the strain sensor attain and even surpass the properties of recent strain sensing devices with subtle design of materials and device architectures. The pen-on-paper (PoP) approach may further develop portable, environmentally friendly, and economical lab-on-paper applications and offer a valuable method to fabricate other multifunctional devices.

1. Introduction

Flexible and wearable sensing devices hold tremendous promise for versatile applications,[1,2] which include but are not limited to electronic skins,[3–5] health monitoring devices,[6–9] flexible displays,[10–12] microfluidic devices,[13] and energy harvesting devices.[14–17] These devices can generate signals under certain environment physical or chemical signals changes, and then operate in a manner.[18–22] In general, they consist of numerous circuits or intricate layered matrix arrays, and are manufactured by complicated producing processes, which lead to an intensive energy consumption and limit their wide applications. By developing the highly efficient, scalable and low-cost fabrication schemes, the flexible functional sensors are competitive and attractive candidates for promoting the advancement of sensing system. Recently, for the achievement of sensing devices, the printing technique has attracted widespread attention and been pursued to deposit various materials, like carbon materials,[13,23,24] polymers,[25,26] metals,[12,27] and semiconductors,[28,29] because the process is low energy consumption while maintaining the unique properties of the materials. By this way, the flexible devices can be cheaper and easily produced.

Graphite, one of carbon allotropes, has been increasing wide and keen interests of researchers, due to a wonder material of graphene.[9,30–32] Pencil, a day-to-day material, is a nanocomposite of graphite and intercalated clay.[33–35] Being layered or pelleted, pencil lead can be exfoliated by using a gentle force. The drawing process can easily deposit graphite onto a rough paper, which contains massive amounts of cellulose fibers and offer a naturally porous structure.[13,36] Pencil-trace drawn on printing papers is perhaps the simplest and easiest way of constructing graphite-based devices. The pen-on-paper (PoP) approach, a basic printing technique, offers a unique method to fabricate flexible devices, such as strain sensors,[35] biosensors,[19,37] microfluidic chips,[38] electronic devices,[34,39] photoconductive sensors,[29,40] and energy-storage devices.[33,41,42] Most of these devices have a response to force-induce changes in capacitance[33] and resistivity.[35] The microcontact-reversible sensing can effectively translate the microstructural deformations into electrical signals on active flexible substrates.[6,9,43,44] As the potential to make flexible, lightweight, portable, biocompatible, economical, and environment-friendly products, the PoP approach has an important role on the breakthroughs toward flexible and wearable sensing devices.

Herein, we demonstrate that the application of PoP approach can be expanded further to crucial flexible sensing devices. We evaluated the repeatability of bending–unbending and the robustness of the strain sensors applied by loading. The strain sensors have a rapid respond to microdeformation changes and can be used to monitor various structural change and even human motion through facilitative and effective installing designs. Typically, the microdeformation of <0.13% strain can be detected. Compared with the recently reported flexible sensing devices, the strain sensors behave significant

Dr. X. Liao, Dr. Q. Liao, Prof. X. Yan, Dr. Q. Liang, Dr. H. Si, Dr. M. Li, Dr. H. Wu, Dr. S. Cao, Prof. Y. Zhang
State Key Laboratory for Advanced Metals and Materials
School of Materials Science and Engineering
University of Science and Technology Beijing
Beijing 100083, P.R. China
E-mail: yuezhang@ustb.edu.cn
Prof. Y. Zhang
Key Laboratory of New Energy Materials and Technologies
University of Science and Technology Beijing
Beijing 100083, P.R. China

DOI: 10.1002/adfm.201500094

advantages of simple and low-cost character as well as quick and convenient fabrication. The strain sensors are wearable, disposable and green products, and even can directly contact with human skin. The PoP approach may be an excellent manufacturing method to grab the attention of researchers, and can be exploited to produce highly flexible, sensitive, and economical lab-on-paper devices.

2. Results and Discussion

Figure 1a describes the fabrication process of the graphite-based device. The device was fabricated by a simple drawing with a graphite pencil on Xerox paper. Figure 1b shows that the device is mechanically robust yet bendable and wearable due to the flexible nature of paper. We know that the printing paper is composed of cellulose fibers and its surface is rough and porous. Moreover, when drawing on the paper with a pencil, the graphite of the pencil can be exfoliated and adhered on the paper. Meanwhile, the surface of the paper can provide a significant penetrative area for large chunks of graphite (Figures 1c, and S1, Supporting Information). The drawing of graphite-pencil deposits a variety of graphite flakes, including multilayer graphenes and small amounts of single-layer graphene with a large portion of edge structures (Figure 1d,e).[45] In addition, the Raman spectrum of a pencil-trace shows the characteristic peaks of graphite and the three prominent peaks at 1350, 1579, and ≈2700 cm^{-1}, which correspond to the *D*, *G*, and 2*D* band, respectively (Figure 1f).[34]

For the accurate fabrication of the device, the ruler-guided drawing on the paper was repeated 10 times in order to form a uniform stripe of pencil-trace film. The variation of resistance *R* of the pencil-trace film was relevant to the drawing times (Figure S2a, Supporting Information).[33] The current–voltage (*I*–*V*) characteristics of the device stated clearly that the pencil-trace on paper could be used as a graphite resistor and it also could be used as a variable resistor to control the brightness of an light-emitting diode (LED) at two batteries voltage of 3V (Figures S2b,S3 and Video 1, Supporting Information). Moreover, the resistance of the graphite resistor varied with the width and length of the pencil-trace. The graphite resistors with different size of the pencil-trace can adjust the brightness of LED at 3 V (Figures S2c,S4 and Video 2, Supporting Information).

In addition to variable resistor, the pencil-trace can be exploited as a strain sensor, as illustrated in **Figure 2**. The sensing principle of the sensor is based on the microcontact-reversible effect of graphite drawn on a paper.[35] As depicted in Figure 2a, we draw a uniform graphite stripe, and two ends of the rectangular silver (Ag) paste were used as contact electrodes. The resistance of the pencil-trace depends on the contact conditions between graphite-slices in the percolative film. The distinct resistance-reversible behaviors of the strain sensors are attributed to amount of contacting areas between graphite-slices with each other. Under tension or compression condition, the strain of the sensor can be efficiently accommodated by the sliding, separating, and rearranging of graphite-slices on the paper but meanwhile a large number of graphite-slices contacting areas are well maintained. By bending the outer surface, the sensor is subjected to tensile stress, which induces an expansion of the cellulose-fiber network on the paper. Subsequently, each graphite-slice was separated and plenty of cracks occur inside pencil-trace film, which lead to increase the resistance of the strain sensor (Figures 2b, 2d, and S5a, Supporting Information). On the contrary, by bending the inner surface, the sensor is subjected to compressive stress. The overlaps of graphite-slices with some microcracks are created when the cellulose-fiber network of the paper are stretched, which lead

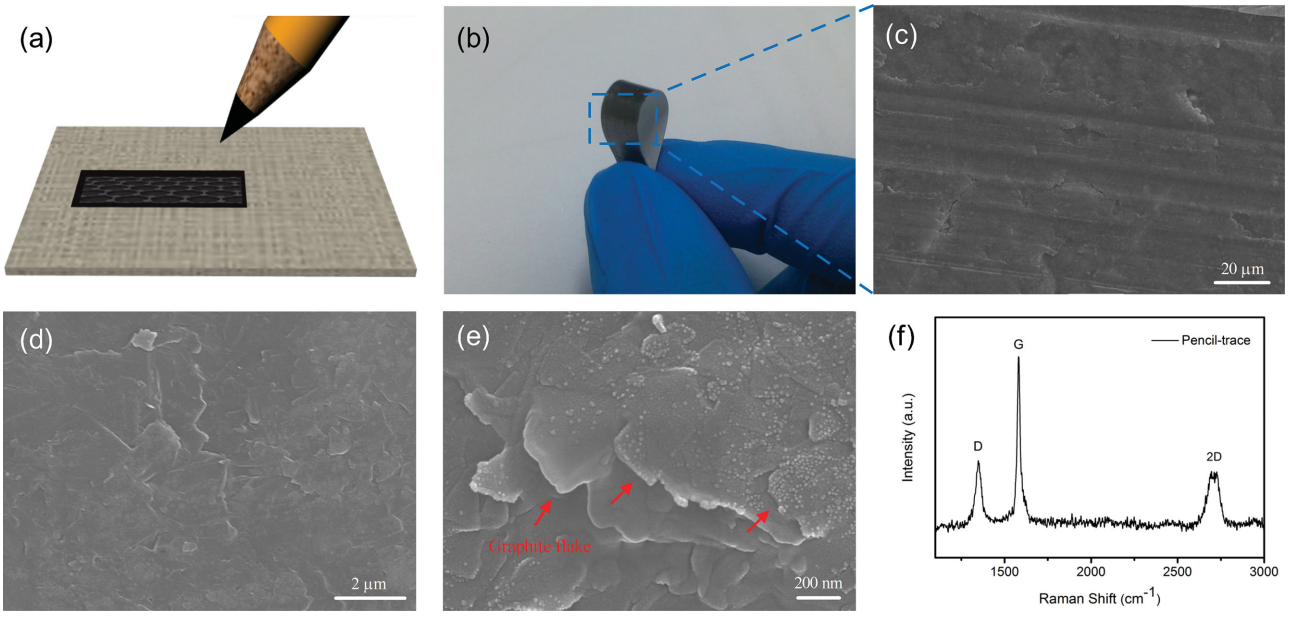

Figure 1. a) Schematic diagram of a pencil-trace drawn on a printing paper to fabricate device. b) Photograph showing the flexibility of the device. c–e) Field emission scanning electron microscopy (FESEM) images of the graphite-coated paper. Red arrows indicate the graphite flakes. f) Raman spectrum of the pencil-trace.

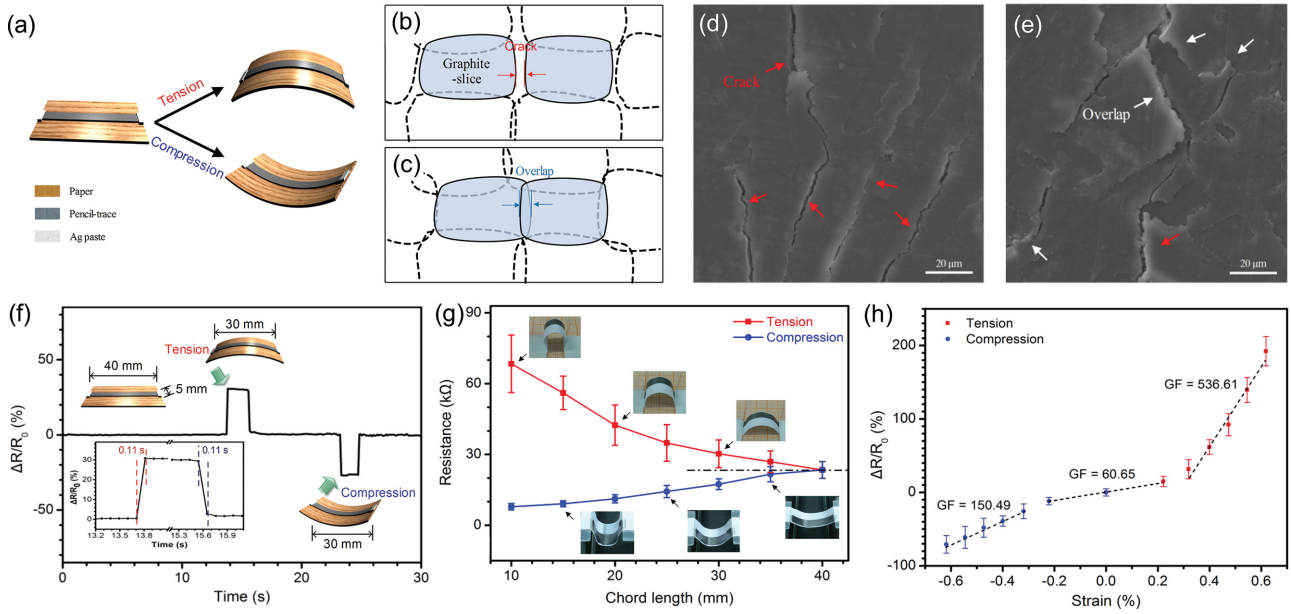

Figure 2. a–c) Schematic illustration of the sensing mechanism. d,e) FESEM images of the graphitic film under tension or compression. Red and white arrows indicate the cracks and overlaps of the graphite-slices, respectively. f) Time response of the sensor applied tensile and compression strain by bending to 30 mm. Inset shows the sensor response time of 110 ms. g) Resistance as functions of the chord length. The red line and blue line are in accordance with the different bending direction [outward deflection (tension) or inward deflection (compression), respectively]. Inset is the optical images of the sensors under different bending states. h) Electrical resistance changes under various strains. GF could be derived by linear fitting.

to decrease the resistance of the strain sensor (Figure 2c,e and S5b, Supporting Information).

In order to evaluate the performance of the strain sensors (width = 5 mm and length = 40 mm), the normalized resistance change ΔR ($=R - R_0)/R_0$, where R and R_0 were the resistances at bending and relaxed state, respectively, was measured in synchrony with the bending of the flexible paper substrate. Figure 2f exhibits the response time of the strain sensor applied by the tensile and compressive stress, respectively when the bending chord length c is about 30 mm. As shown in the inset of Figure 2f, the strain sensor exhibits immediate response time of ≈110 ms under tension and compression condition, which is slower than the response time (17 ms) of gold nanowires devices,[6] and favorably comparable with recent values of other nanocomposite sensors (90–200 ms),[26,27,43] and faster than the time of the previously reported (300–3800 ms).[46–48] Furthermore, the response time of the strain sensor is so sufficient to be used to structural health monitoring systems, wearable sensors and robotic applications.

To investigate the mechanical flexibility of the strain sensor, we take the average R values measured by five tests as a function of chord length of the bending strain sensor (Figure 2g). The output resistance of the strain sensor was modulated by seven values of the chord length: 40 → 35 → 30 → 25 → 20 → 15 → 10 mm, and the resistance of the strain sensor depends on the different bending direction. The resistance increases or decreases when the bending direction is outward (tension) or inward (compression), respectively. The behavior of the strain sensor can directly detect the direction of bending. We know that chord length c has a relationship with curvature radius r as: $c = 2r^*\sin(l/2r)$, where l is the arc length of the sensor under bending state. On the contrary, the strain ε of the sensor can be expressed as: $\varepsilon = \pm h/2r$, where h is the thickness (≈100 μm) of the sensor (see Figure S6, Supporting Information). Thus, the relationship between the resistivity and strain for the strain sensor can be derived from Figure 2g. As displayed in Figure 2h, the strain sensor is very sensitive under both tensile and compressive strain. Moreover, the gauge factor GF = $(\Delta R/R_0)/\Delta\varepsilon$ is higher under tensile strain than the value under compressive strain, due to the exponential dependence of relative resistance variation.[49] Some small cracks on the pencil-trace film may weaken the sensitivity of the strain sensor under compressive strain (Figure 2e). For the relatively small strain (between –0.22% and 0.22% strain), the GF (≈60.6) of the strain sensor is lower. The result is due to the sliding of graphite-slices, the microseparating and microrearranging of contacting areas between graphite-slices (Figure S5, Supporting Information). In the range from –0.62% to –0.32% and from 0.32% to 0.62% strain, respectively the GFs are from 150.5 to 536.6. These higher GFs are attributed to the generated larger cracks or overlaps of contacting areas between graphite-slices (Figure 2d,e). The maximum magnitude of GF is about 536.6, which indicates the strain sensors are indeed much more sensitive. Generally, the GF values of the conventional metal foil strain sensors and semiconductor ones are about 2 and 50, respectively. Though the GF value is lower than that of carbon nanotube sensor (600–1000),[50] it is obvious higher than that of the recent other sensors (4.4–116).[6,9,14,24,27,51]

Then, to examine the mechanical robustness and the reliability of the strain sensors, we subjected them to multibending cycles under both tensile and compressive modes, and obtained the normalized resistance change (**Figure 3**). As presented in Figure 3a,b, the strain sensors were bended and released repeatedly under ±0.22% and ±0.32% strain. A stable response

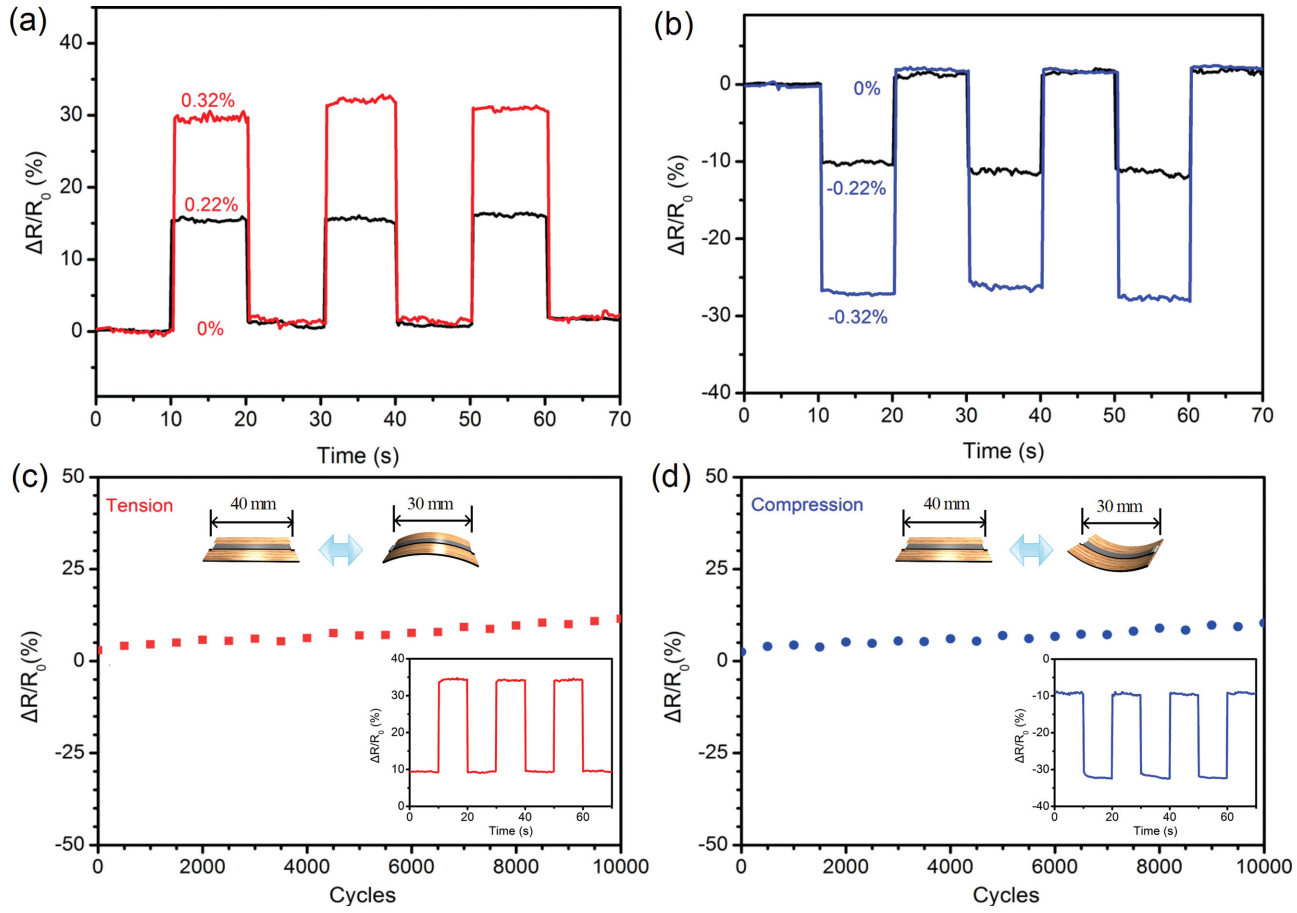

Figure 3. a,b) The normalized resistance change subjected multibending under both tensile (0.22% and 0.32% strain) and compressive (–0.22% and –0.32% stain) modes at cycle strain. Mechanical reliability of the normalized resistance change after c) tensile and d) compressive bending cycles at ±0.32% strain. Insets of (c) and (d) are the sensors response under ±0.32% strain condition after 10 000 bending cycles.

of the strain sensors were observed with a small passive upward drift of the resistance at rest state under each cycle regardless of tension or compression state, due to the cracks generated in the smooth pencil-trace film. We also performed multiple cycle tests (≈10 000 cycles) of the strain sensors repeatedly applied by ≈0.32% strain and relaxed, following by measuring the resistance values of the strain sensors under the relaxed state. As shown in Figure 3c,d, the resistance values of the strain sensors irreversibly ranged from 1.18% to 10.33% for tension, and from 1.05% to 9.72% for compression, both caused by increasing microcracks under relaxed state. After such cycle tests, we further examined the responses of the strain sensors. The strain sensors also can respond stably, as illustrated in insets of Figure 3c,d. These results present that the strain sensors feature well tenability and mechanical flexibility.

Next, we explored the sensitivity of the strain sensor, which can be used to monitor the microstrain structural variation (**Figure 4**). We stuck the sensor to a flexible structure surface in order to detect the tensile and compressive strain deformation (±0.13%), as exhibited in Figure 4a–c. The change in resistance was expressed as normalized values against strain (Figure 4d,e). Remarkably, the two response curves are characteristic for the two kinds of mechanical deformation on the same strain sensor (Video 3,4, Supporting Information). High signal-to-noise ratios of the strain sensor were measured, which demonstrated the pencil-trace sensor had higher sensitivity. These results indicate that the strain sensors have the potential application for structural health monitoring systems, such as monitoring the state of buildings, bridges, and other critical infrastructures under severe natural disasters in real time.

We also examined the pencil-trace sensor as a folding-type sensing device, which is fixed in the folding line of a book (**Figure 5**). In detail, the electromechanical properties of the sensor were investigated by measuring the resistance at the different angles θ (Figure 5a,b). We checked the resistance variation of the folding-type sensor by opening the book at 20°, 45°, 70°, 90°, and 130° step by step (each step was held for several seconds) and then closing gradually from 130° to 90°, 70°, 45°, and 20°. The relative change in resistance increased with opening book from 20° to 130° (tensile strain) and decreased with closing book from 130° to 20° (compressive strain), as presented in Figure 5c and Video 5 (Supporting Information). Notably, the folding-type sensor responded rapidly at each turning angle and the resistance remained identical under the same angle. Similarly, this folding-type sensor allows us to measure the changes of robotic joints angles instead of

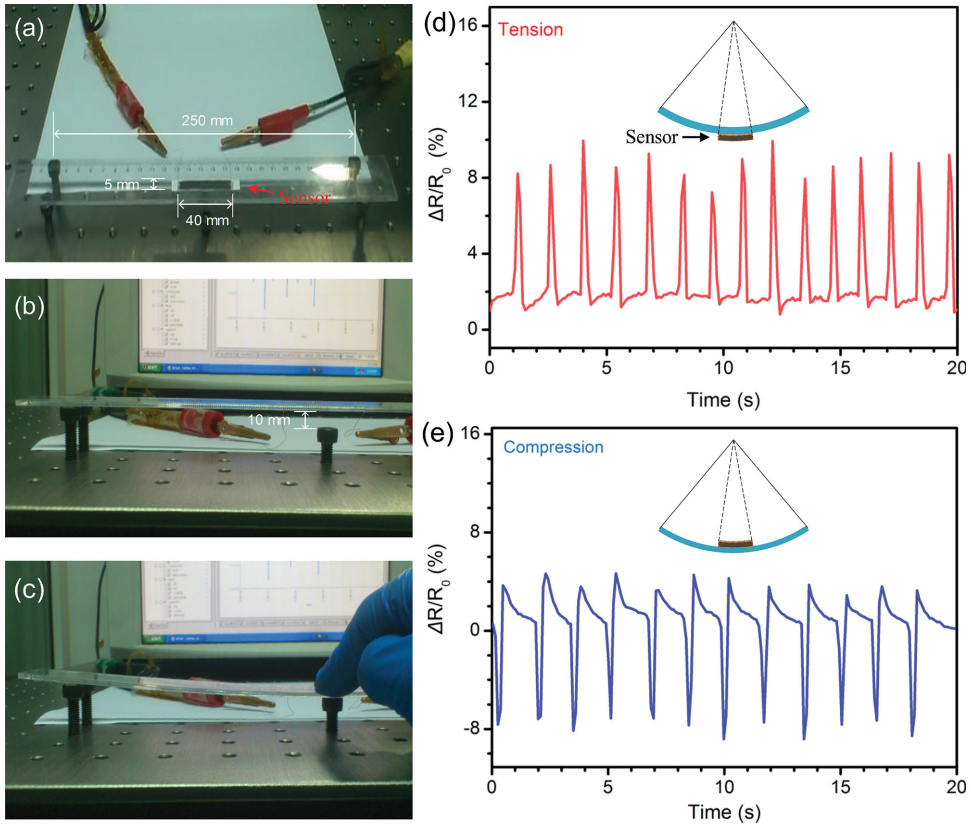

Figure 4. a–c) Photographs of a sensor fixed to a flexible surface in order to detect microstrain structural variation. d,e) Relative changes in resistance for the tensile and compressive strain (±0.13%). Inset to the monitoring models of d) tension and e) compression.

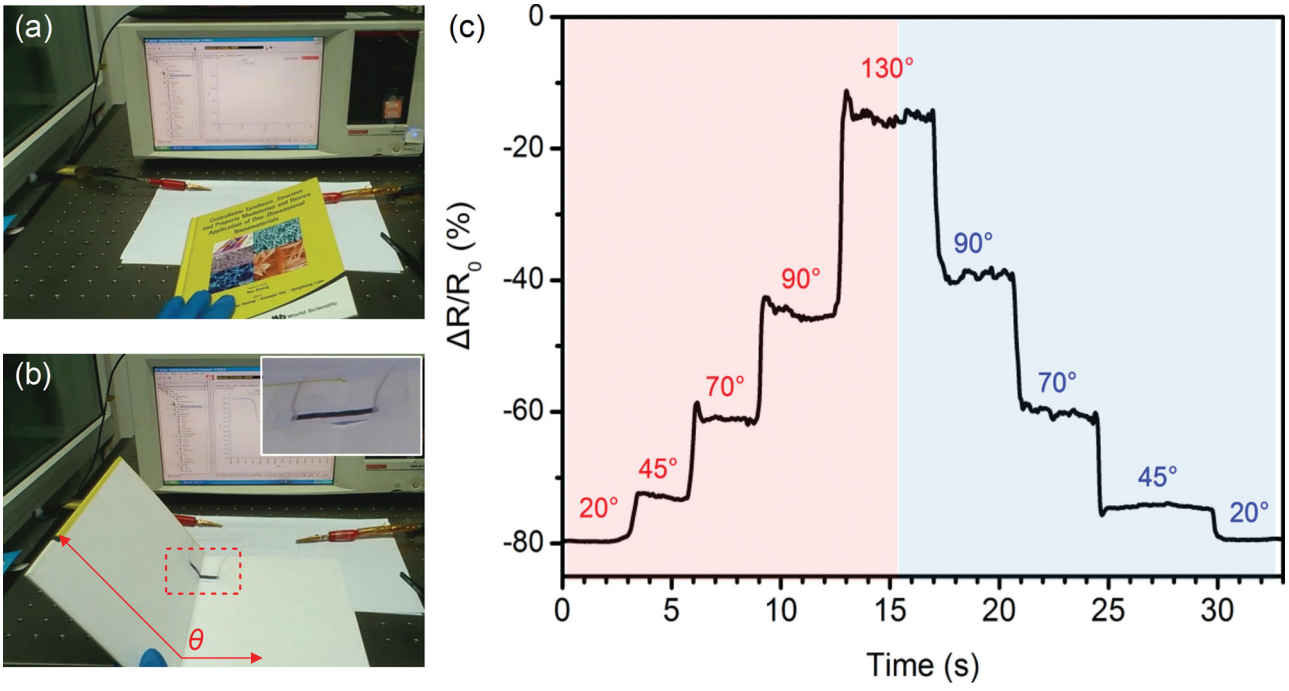

Figure 5. a,b) Photographs of a folding-type sensor fixed in the folds of a book. Inset to (b) close-up of the strain sensor. c) The resistance variation of the sensor under closing (red area) and opening (blue area) the book states.

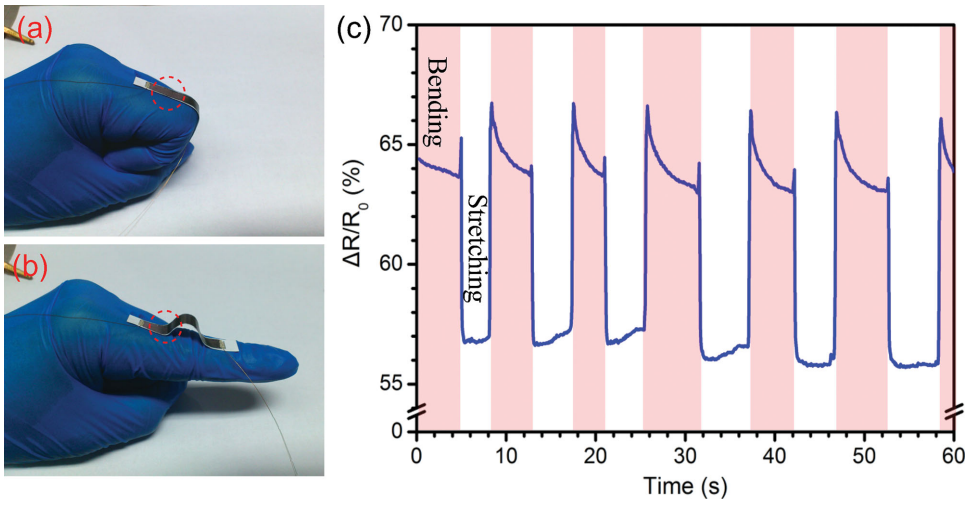

Figure 6. a,b) Photographs of a wearable sensor attached onto a forefinger for monitoring human-motion. The red dotted line circles show the deformation areas of the sensor under bending and stretching states of the finger. c) Relative resistance changes during the finger bending tests.

encoders. In essence, the results indicate that the strain sensors have attractive perspective applications for robotics and the opening/closing states of the doors for the multifunctional intelligent room system.

We further investigated the behaviors of the flexible strain sensor for human-motion detection, which have an extensive attraction for the smart robots and wearable electronic devices (**Figure 6**). As fingers undertook many sophisticated human actions, we attached the strain sensor onto a forefinger for the potential application in wearable electronics, as displayed in Figure 6a,b, and Video 6 (Supporting Information). For each bending-stretching motion of the finger, the strain sensor responded rapidly and repeatedly. The results were primarily due to a part (as inside the red dotted line circles in Figure 6a,b) of the strain sensor under a relaxed or compressive state without regarding to the trembling of the finger. The results indicate that the strain sensors are able to monitor different parts of the human body motions and are suitable to wearable devices and human-machine interfacing applications.

3. Conclusion

In summary, we report a simple and convenient method for the fabrication of flexible, robust, portable, environment-friendly and economical (<$0.1/sensor) variable resistors and strain sensors based on graphite and printing papers. The prototype devices can be fabricated rapidly (<5 min for full assembly) with minimal equipment, and provide an attractive option according to somebody's need. Notably, the strain sensors feature an impressively high GFs of ≈150.5 (compressive strain <–0.32%), ≈60.7 (between –0.22% and 0.22% strain) and ≈536.6 (tensile strain >0.32%) in the strain range from –0.62% to 0.62% under compressive and tensile bending conditions, which are fairly comparable to or superior to recent studies of other sensors. The different GFs of the strain sensors are attributed to the sliding of graphite-slices and the separating or rearranging between graphite-slices of the pencil-trace on the paper. Through researching the service behaviors of the sensors by multiple bending cycle tests (>10 000 cycles), the strain sensors allow a simple sensing platform for the high repeatable output signals at ±0.32% strain within relative resistance variability of 10.33%. Interestingly, the sensors are able to monitor the microstrain (<0.13%) structural variation, book-folding (similarly, the changes of robotic joints angles and the opening/closing states of the doors for multifunctional intelligent room system), and human motion with fast response time of <110 ms. We believe that the designs and operational principles of the devices present a feasible, facilitative, and robust technology platform for the wide applications of various multifunctional electric devices with optimal performances.

4. Experimental Section

Preparation of the Strain Sensor: Graphite-pencil (2B) drawing with ruler-guided in orthogonal direction was repeated 10 times to form a stripe of uniform coating film on a Xerox paper. The pencil-trace is 5 mm width and 40 mm length. Then two ends of the rectangular silver (Ag) paste were used as contact electrodes to lead to the conductive line.

Characterization: Field emission scanning electron microscope (FESEM, SUPRA55) was employed to observe the morphology of synthesized materials. The Raman spectrum was obtained by utilizing confocal Raman spectroscopy (JY-HR800) with an Ar^+ laser source at room temperature. The electromechanical properties of the strain sensors were measured with semiconductor characterization system (Keithley 4200).

Supporting Information

Supporting Information is available from the Wiley Online Library or from the author.

Acknowledgements

This work was supported by the National Major Research Program of China (Grant No. 2013CB932602), the Major Project of International

Cooperation and Exchanges (Grant No. 2012DFA50990), the Program of Introducing Talents of Discipline to Universities (Grant No. B14003), National Natural Science Foundation of China (NSFC) (Grant Nos. 51232001, 51172022, 51372020, and 51372023), the Fundamental Research Funds for Central Universities, the Research Fund of Coconstruction Program from Beijing Municipal Commission of Education, Program for New Century Excellent Talents in Universities, and the Program for Changjiang Scholars and Innovative Research Teams in Universities.

Received: January 8, 2015
Revised: February 11, 2015
Published online: March 11, 2015

[1] J. A. Rogers, T. Someya, Y. Huang, *Science* **2010**, *327*, 1603.
[2] Y. Zang, F. Zhang, C. A. Di, D. Zhu, *Mater. Horiz.* **2015**, *2*, 140.
[3] D. H. Kim, N. Lu, R. Ma, Y. S. Kim, R. H. Kim, S. Wang, J. Wu, S. M. Won, H. Tao, A. Islam, K. J. Yu, T. I. Kim, R. Chowdhury, M. Ying, L. Xu, M. Li, H. J. Chung, H. Keum, M. McCormick, P. Liu, Y. W. Zhang, F. G. Omenetto, Y. Huang, T. Coleman, J. A. Rogers, *Science* **2011**, *333*, 838.
[4] M. L. Hammock, A. Chortos, B. C. Tee, J. B. Tok, Z. Bao, *Adv. Mater.* **2013**, *25*, 5997.
[5] M. Kaltenbrunner, T. Sekitani, J. Reeder, T. Yokota, K. Kuribara, T. Tokuhara, M. Drack, R. Schwodiauer, I. Graz, S. Bauer-Gogonea, S. Bauer, T. Someya, *Nature* **2013**, *499*, 458.
[6] S. Gong, W. Schwalb, Y. Wang, Y. Chen, Y. Tang, J. Si, B. Shirinzadeh, W. Cheng, *Nat. Commun.* **2014**, *5*, 3132.
[7] G. Schwartz, B. C. Tee, J. Mei, A. L. Appleton, H. Kim do, H. Wang, Z. Bao, *Nat. Commun.* **2013**, *4*, 1859.
[8] T. Yamada, Y. Hayamizu, Y. Yamamoto, Y. Yomogida, A. Izadi-Najafabadi, D. N. Futaba, K. Hata, *Nat. Nanotechnol.* **2011**, *6*, 296.
[9] C. Yan, J. Wang, W. Kang, M. Cui, X. Wang, C. Y. Foo, K. J. Chee, P. S. Lee, *Adv. Mater.* **2014**, *26*, 2022.
[10] M. S. White, M. Kaltenbrunner, E. D. Głowacki, K. Gutnichenko, G. Kettlgruber, I. Graz, S. Aazou, C. Ulbricht, D. A. M. Egbe, M. C. Miron, Z. Major, M. C. Scharber, T. Sekitani, T. Someya, S. Bauer, N. S. Sariciftci, *Nat. Photonics* **2013**, *7*, 811.
[11] C. Wang, D. Hwang, Z. Yu, K. Takei, J. Park, T. Chen, B. Ma, A. Javey, *Nat. Mater.* **2013**, *12*, 899.
[12] J. Liu, C. Yang, H. Wu, Z. Lin, Z. Zhang, R. Wang, B. Li, F. Kang, L. Shi, C. P. Wong, *Energy Environ. Sci.* **2014**, *7*, 3674.
[13] H. Ko, J. Lee, Y. Kim, B. Lee, C. H. Jung, J. H. Choi, O. S. Kwon, K. Shin, *Adv. Mater.* **2014**, *26*, 2335.
[14] Q. Liao, M. Mohr, X. Zhang, Z. Zhang, Y. Zhang, H. J. Fecht, *Nanoscale* **2013**, *5*, 12350.
[15] Q. Liao, Z. Zhang, X. Zhang, M. Mohr, Y. Zhang, H.-J. Fecht, *Nano Res.* **2014**, *7*, 917.
[16] J. Chun, N.-R. Kang, J.-Y. Kim, M.-S. Noh, C.-Y. Kang, D. Choi, S.-W. Kim, Z. Lin Wang, J. Min Baik, *Nano Energy* **2015**, *11*, 1.
[17] G. Zhou, L. Li, C. Ma, S. Wang, Y. Shi, N. Koratkar, W. Ren, F. Li, H.-M. Cheng, *Nano Energy* **2015**, *11*, 356.
[18] Y. Yang, W. Guo, J. Qi, Y. Zhang, *Appl. Phys. Lett.* **2010**, *97*, 223107.
[19] K. A. Mirica, J. G. Weis, J. M. Schnorr, B. Esser, T. M. Swager, *Angew. Chem. Int. Ed.* **2012**, *51*, 10740.
[20] Y. Zhang, X. Yan, Y. Yang, Y. Huang, Q. Liao, J. Qi, *Adv. Mater.* **2012**, *24*, 4647.
[21] Y. Yang, W. Guo, X. Wang, Z. Wang, J. Qi, Y. Zhang, *Nano Lett.* **2012**, *12*, 1919.
[22] Z. Zhang, Q. Liao, X. Yan, Z. L. Wang, W. Wang, X. Sun, P. Lin, Y. Huang, Y. Zhang, *Nano Res.* **2013**, *7*, 190.
[23] X. Liu, M. Mwangi, X. Li, M. O'Brien, G. M. Whitesides, *Lab Chip* **2011**, *11*, 2189.
[24] J. T. Muth, D. M. Vogt, R. L. Truby, Y. Menguc, D. B. Kolesky, R. J. Wood, J. A. Lewis, *Adv. Mater.* **2014**, *26*, 6307.
[25] C. Chang, V. H. Tran, J. Wang, Y. K. Fuh, L. Lin, *Nano Lett.* **2010**, *10*, 726.
[26] S. Harada, W. Honda, T. Arie, S. Akita, K. Takei, *ACS Nano* **2014**, *8*, 3921.
[27] K. Takei, Z. Yu, M. Zheng, H. Ota, T. Takahashi, A. Javey, *Proc. Natl. Acad. Sci. USA* **2014**, *111*, 1703.
[28] H. Minemawari, T. Yamada, H. Matsui, J. Tsutsumi, S. Haas, R. Chiba, R. Kumai, T. Hasegawa, *Nature* **2011**, *475*, 364.
[29] K. ul Hasan, O. Nur, M. Willander, *Appl. Phys. Lett.* **2012**, *100*, 211104.
[30] A. K. Geim, *Science* **2009**, *324*, 1530.
[31] L. Liao, H. Peng, Z. Liu, *J. Am. Chem. Soc.* **2014**, *136*, 12194.
[32] J. U. Park, S. Nam, M. S. Lee, C. M. Lieber, *Nat. Mater.* **2012**, *11*, 120.
[33] G. Zheng, L. Hu, H. Wu, X. Xie, Y. Cui, *Energy Environ. Sci.* **2011**, *4*, 3368.
[34] N. Kurra, D. Dutta, G. U. Kulkarni, *Phys. Chem. Chem. Phys.* **2013**, *15*, 8367.
[35] C. W. Lin, Z. Zhao, J. Kim, J. Huang, *Sci. Rep.* **2014**, *4*, 3812.
[36] L. Liu, Z. Niu, L. Zhang, W. Zhou, X. Chen, S. Xie, *Adv. Mater.* **2014**, *26*, 4855.
[37] R. K. Arun, S. Halder, N. Chanda, S. Chakraborty, *Lab Chip* **2014**, *14*, 1661.
[38] M. M. Thuo, R. V. Martinez, W.-J. Lan, X. Liu, J. Barber, M. B. J. Atkinson, D. Bandarage, J.-F. Bloch, G. M. Whitesides, *Chem. Mater.* **2014**, *26*, 4230.
[39] A. Russo, B. Y. Ahn, J. J. Adams, E. B. Duoss, J. T. Bernhard, J. A. Lewis, *Adv. Mater.* **2011**, *23*, 3426.
[40] L. Polavarapu, A. L. Porta, S. M. Novikov, M. Coronado-Puchau, L. M. Liz-Marzan, *Small* **2014**, *10*, 3065.
[41] Y. Wang, H. Zhou, *Energy Environ. Sci.* **2011**, *4*, 1704.
[42] B. Yao, L. Yuan, X. Xiao, J. Zhang, Y. Qi, J. Zhou, J. Zhou, B. Hu, W. Chen, *Nano Energy* **2013**, *2*, 1071.
[43] C. L. Choong, M. B. Shim, B. S. Lee, S. Jeon, D. S. Ko, T. H. Kang, J. Bae, S. H. Lee, K. E. Byun, J. Im, Y. J. Jeong, C. E. Park, J. J. Park, U. I. Chung, *Adv. Mater.* **2014**, *26*, 3451.
[44] D. Kang, P. V. Pikhitsa, Y. W. Choi, C. Lee, S. S. Shin, L. Piao, B. Park, K.-Y. Suh, T.-i. Kim, M. Choi, *Nature* **2014**, *516*, 222.
[45] K. S. Novoselov, D. Jiang, F. Schedin, T. J. Booth, V. V. Khotkevich, S. V. Morozov, A. K. Geim, *Proc. Natl. Acad. Sci. USA* **2005**, *102*, 10451.
[46] M. Ramuz, B. C. Tee, J. B. Tok, Z. Bao, *Adv. Mater.* **2012**, *24*, 3223.
[47] K. Sun, J. Qi, Q. Zhang, Y. Yang, Y. Zhang, *Nanoscale* **2011**, *3*, 2166.
[48] Z. Wang, J. Qi, X. Yan, Q. Zhang, Q. Wang, S. Lu, P. Lin, Q. Liao, Z. Zhang, Y. Zhang, *RSC Adv.* **2013**, *3*, 17011.
[49] C. Farcau, N. M. Sangeetha, H. Moreira, B. Viallet, J. Grisolia, D. Ciuculescu-Pradines, L. Ressier, *ACS Nano* **2011**, *5*, 7137.
[50] J. Cao, Q. Wang, H. Dai, *Phys. Rev. Lett.* **2003**, *90*, 157601.
[51] X. Xiao, L. Yuan, J. Zhong, T. Ding, Y. Liu, Z. Cai, Y. Rong, H. Han, J. Zhou, Z. L. Wang, *Adv. Mater.* **2011**, *23*, 5440.